




Article

Process Mineralogy of the Tailings from Llallagua: Towards a Sustainable Activity

Pura Alfonso ^{1,*} , Miguel Ruiz ², Rubén Néstor Zambrana ³, Miquel Sendrós ¹, Maite Garcia-Valles ⁴ , Hernan Anticoi ⁵ , Nor Sidki-Rius ¹ and Antonio Salas ²

- ¹ Departament d'Enginyeria Minera, Industrial i TIC, Universitat Politècnica de Catalunya Barcelona Tech, Av. Bases de Manresa 61-63, 08242 Manresa, Barcelona, Spain; msendros@upc.edu (M.S.); nor.sidki@upc.edu (N.S.-R.)
- ² Facultad Nacional de Ingeniería, Universidad Técnica de Oruro, Ciudadela Universitaria, Oruro 0401, Bolivia; miguelruiz@mecanica.edu.bo (M.R.); antoniosalas@metalurgia.edu.bo (A.S.)
- ³ Tecnología, Campus Universitario María Barzola, Universidad Nacional Siglo XX, Llallagua 0502, Bolivia; rubennzm@gmail.com
- ⁴ Departament de Mineralogia, Petrologia i Geologia Aplicada, Universitat de Barcelona, Carrer Martí i Franquès, s/n, 08028 Barcelona, Spain; maitegarciavalles@ub.edu
- ⁵ Grupo de Investigación de Ingeniería Cartográfica y Explotación de Minas, Escuela Politécnica de Ingeniería de Minas y Energía, Universidad de Cantabria, Bvd Ronda Rufino Peón, 254, Tanos, 39300 Torrelavega, Spain; hernan.anticoi@upc.edu
- * Correspondence: maria.pura.alfonso@upc.edu

Abstract: There are significant tin reserves in the dumps and tailings from Llallagua. Currently, this waste is being processed using gravity concentration or a combination of gravity concentration with a final stage of froth flotation. A process mineralogy study of the tailings and their products after processing in Llallagua was carried out to determine the failings of the processing system in order to contribute to designing an improved new processing scheme. The mineralogy of the feed tailings, concentrate, and final tailings was determined by X-ray diffraction, scanning electron microscopy, and mineral liberation analysis. The tailings were composed of quartz, tourmaline, illite, K-feldspar, plagioclase, cassiterite, rutile, zircon, and monazite. The concentrate essentially contains cassiterite (57.4 wt.%), tourmaline, quartz, hematite, rutile and rare earth minerals, mainly monazite and minor amounts of xenotime and florencite. The concentrate contained 52–60 wt.% of SnO₂ and 0.9–1.3 wt.% REE. The final tailings contained 0.23–0.37 wt.% SnO₂ and 0.02 wt.% of Rare Earth Elements (REE). Only 57.6 wt.% of cassiterite from the concentrate was liberated. The non-liberated cassiterite was mainly associated with quartz, tourmaline, and rutile. The average grain size of monazite was 45 µm and 57.5 wt.% of this was liberated. In other cases, it occurs in mixed particles associated with tourmaline, quartz, cassiterite, and muscovite. To improve the sustainability of this mining activity, the concentrate grade and the metal recovery must be improved. Reducing the particle size reduction of the processed tailings would increase the beneficiation process rates. In addition, the recovery of the REE present in the concentrate as a by-product should be investigated.

Keywords: process mineralogy; tailings; cassiterite; REE; mineral liberation; quantitative mineralogy



Citation: Alfonso, P.; Ruiz, M.; Zambrana, R.N.; Sendrós, M.; Garcia-Valles, M.; Anticoi, H.; Sidki-Rius, N.; Salas, A. Process Mineralogy of the Tailings from Llallagua: Towards a Sustainable Activity. *Minerals* **2022**, *12*, 214. <https://doi.org/10.3390/min12020214>

Academic Editors: Shenghua Yin and Leiming Wang

Received: 14 December 2021

Accepted: 5 February 2022

Published: 7 February 2022

Publisher's Note: MDPI stays neutral with regard to jurisdictional claims in published maps and institutional affiliations.



Copyright: © 2022 by the authors. Licensee MDPI, Basel, Switzerland. This article is an open access article distributed under the terms and conditions of the Creative Commons Attribution (CC BY) license (<https://creativecommons.org/licenses/by/4.0/>).

1. Introduction

At present, much attention is being paid to the inefficiency of mining activities, which produces large amounts of environmental pollution. Approximately 5 to 7 billion tons of mine tailings are generated each year [1]. Their environmental impact is considerable since, in addition to occupying large areas, they can emit potentially toxic elements [2]. For this reason, mining should be carried out in a more sustainable way. Although there are different concepts of what is considered to be sustainable mining [3], it is generally described as mining that minimizes environmental impacts, operates with a social license, produces economic gains, and focuses on safety and resource efficiency [4]. Therefore,

sustainable mining must optimize resources in addition to preventing environmental pollution [5,6].

The mining activities related to the Siglo XX mine, located in Llallagua (Bolivia), are a clear example of a low sustainable mining. As a result of the mining operations, the tin reserves from Llallagua are found both in an ore deposit and in the waste produced from the extraction and processing of the primary ores.

The Llallagua tin deposit began to be exploited on a large scale at the beginning of the 20th century with the extraction of high-grade tin ores. This mine, also called La Salvadora, was considered the richest tin mine in the world in the last century. There are no contemporary estimates, but the Llallagua tin production reached more than 500,000 tons between the beginning of the 20th century and 1930s [7], and low-grade resources of approximately 1,000,000 t of tin [7,8] have been reported. Initially, certain veins contained more than 25% cassiterite, but currently, veins contain less SnO_2 [9]. Additionally, 20.7 million tons of dumps and tailings were produced as a result of the Llallagua mine, with an average of 0.3% SnO_2 [10]. According to Villalpando [11], 300,000 t of tin reserves remain in placers, dumps, and tailings in Bolivia.

The residues from Llallagua are reprocessed, and even the newly generated tailings are tin-rich, i.e., of economic interest. This makes this mining area a clear example of an unsustainable operation. A great deal of energy is expended to mine the tin ores with a consequent low recovery rate, generating tailings that can be reprocessed. The environmental costs of generating and handling such large quantities of materials, which are rich in potentially toxic elements, are great. In addition to causing economic losses, low efficiency processes have an impact on environmental pollution, since a low recovery rate indicates that metals remain in the final tailings and, consequently, end up in the environment. The pollution created by the Llallagua waste is significant and, for example, the Catavi river receives As [12].

Currently, the Llallagua mining activities represent an important contribution to the Bolivian economy. The mine is mainly operated through mining cooperatives, the most important being the Multiactiva Catavi Ltd. Cooperative (Llallagua, Bolivia), which has been operating since 1986. Approximately 38% of the population in the area is exclusively dedicated to mining activities.

The aim of this work was to provide an example of unsustainable mining activities and show how processing mineralogy can contribute to identifying weaknesses in processing systems and help to improve them. To this end, process mineralogy was carried out using tailings from the Catavi plant of the Llallagua mine. The study could be used to revise and modify the current system of operation, making it more efficient, improving the recovery rates, and making it more environmentally friendly.

Another important motivation to conduct an exhaustive characterization of processing materials in the Llallagua mine is that they contain abundant rare earth-rich minerals, mainly monazite [13–16]. Rare earth elements (REE) are considered to be essential raw materials, especially in key fields, such as the development of clean technologies [17] Zhou. The extreme dependence on China, which is the main provider of these elements, makes them critical for many countries [18,19]. Thus, it is necessary to extract them from different sources, such as tailings [20], where they can be found in relative abundance and recovered as a by-product from certain mining processes [21].

2. Materials and Methods

2.1. Materials

The investigated tailings are the result of the processing of the run-off-mine materials from the Llallagua ore deposit, in the department of Potosí, Bolivia. This deposit belongs to a major tin district located in the Central Andean tin belt (Figure 1a). The exploited deposit is of the porphyry type and it occurs in association with the quartz-dioritic to rhyodacitic La Salvadora stock of Lower Miocene age, intruded in Silurian sedimentary rocks [22,23]. Most parts of this stock are composed of hydrothermal breccia [24] and the mineraliza-

tion is cassiterite, which occurs in veins and is disseminated in the stock [22,24,25]. The mineralization occurred in two stages: in the first stage, cassiterite pyrrhotite, tourmaline, bismuthinite, fluorapatite, and monazite were formed; in the second, late sulfides were superimposed to the early formed mineralization [22,26].



Figure 1. (a) Location of Llalagua in the Central Andean tin belt. Data from [27]; (b) View of Llalagua city and the mining wastes: A, dumps; B, sand tailings; and C, fine tailings.

Monazite can be very abundant as it is associated with the mineralization of cassiterite veins [15]. The stock is highly altered and almost all of the original feldspars have been transformed. Alteration includes sericitization and tourmalinization [22].

The dumps and tailings produced as a consequence of the exploitation of the Llalagua deposit cover a vast area close to the city (Figure 1b), with an estimation of about 18 Mt of tailings and 1.2 of dumps [10].

The investigated tailings are processed in the C-4 treatment plant located in Catavi, close to Llalagua. The supply of this plant corresponds to three types of materials: (1) those that come directly from the La Salvadora mine. (2) large dumps formed by the removal of waste material in order to reach the mineralized zone; and (3) tailings constituted by sands and fine materials resulted from previous processing of the ores. The plant processes about 250 t/day, obtaining about 1 t of concentrate with 51–57% SnO_2 [10].

At the plant (Figures 2 and 3), the tailing sands are initially introduced into ball mills for size reduction. Then, they are transported to a hydraulic classifier. From here, the +250 μm material is returned to the ball mill and the −250 μm material is fed through several shaking tables, separating the high-density minerals from the lighter minerals that constitute the new tailings. Finally, the first concentrate follows two different routes: If it is rich in sulfides, it is subjected to flotation, where these minerals are removed and a final concentrate is obtained. In other cases, to increase the grade of the concentrate, it passes from the shaking tables to a hydrocyclone; from there, it is further ground in a ball mill and finally passed through another shaking table to obtain the final concentrate.

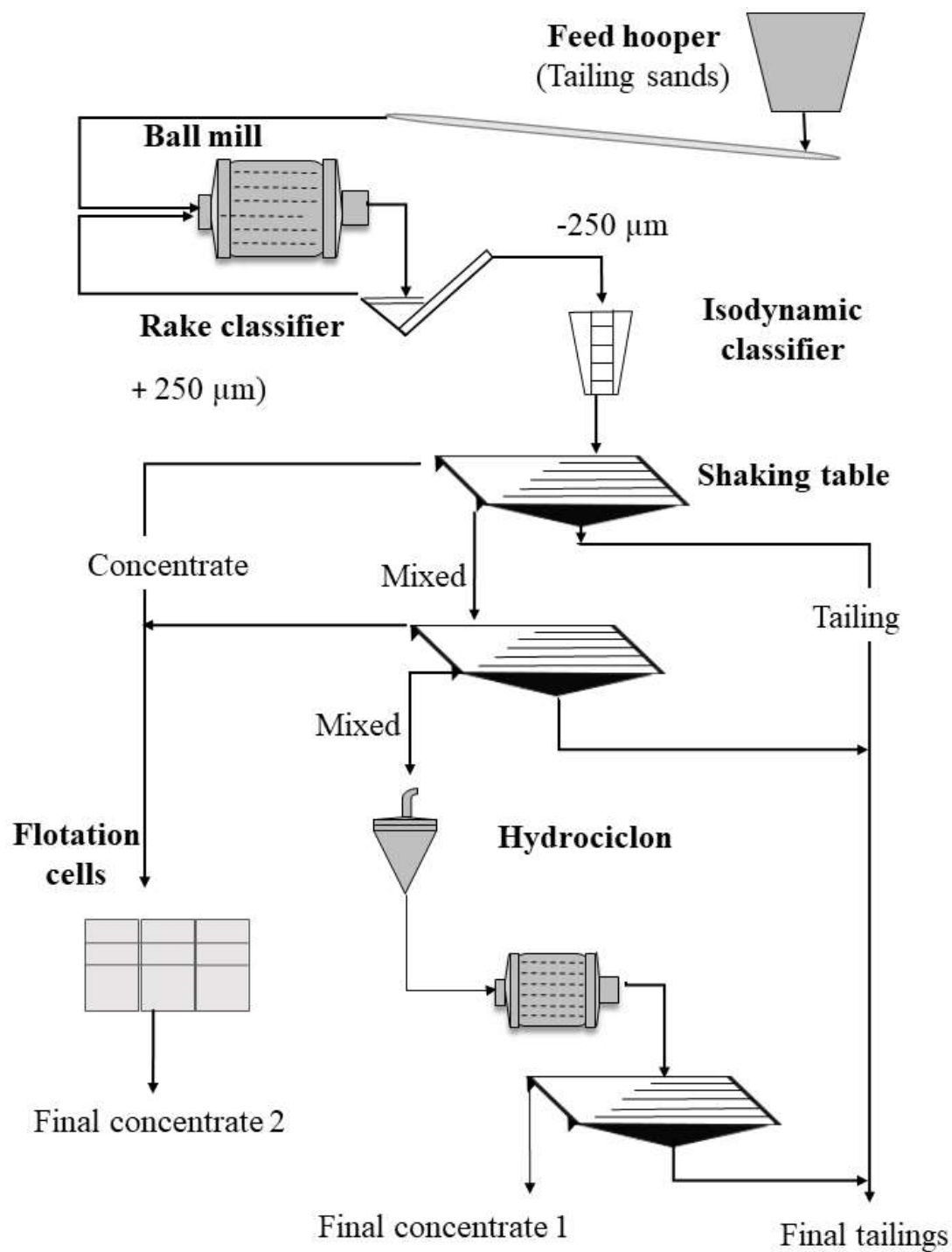


Figure 2. Simplified flux diagram followed by the samples used in this study in the Catavi processing plant.

The residual solid material is sent to waste piles located in the vicinity of the plant, while the liquid is removed using a gutter that empties directly into the river.

The samples used in this study were as follows: the sandy tailings that constitute the feed material of the processing plant; concentrate 1, which had been subjected to flotation; concentrate 2, which had not been floated; an intermediate concentrate; and the final tailings.



Figure 3. View of the Catavi processing plant: (a) feed tailings; (b) ball mill for the comminution; (c), view of one of the three floors with the material being processed in the shaking tables; (d), detail of the gravity separation in a shaking table.

2.2. Methods

The chemical composition of major elements and traces was determined. Major elements were analyzed by X-ray fluorescence (XRF) using a sequential X-Ray PW2400 spectrophotometer (Philips, Amsterdam, The Netherlands) located at the Centres Científics i Tecnològics de la Universitat de Barcelona. Traces and Sn were determined at the ALS Laboratories. Minor elements were measured using ICP-MS from the acid digestion of fused glass beads. Sn was determined by XRF. Fusion was obtained using lithium or sodium borate.

The particle size distribution of the tailings and concentrate was determined using a LS 13 320 Particle Size Analyzer (Beckman Coulter, Brea, CA, USA). Before being measured, the samples were treated with sodium pyrophosphate and mechanically agitated for 24 h in order to achieve complete disaggregation.

Mineralogical characterization was carried out by X-ray powder diffraction (XRD), optical and scanning electron microscopy. The XRD spectra were measured from powdered samples in a Bragg–Brentano PANalytical X’Pert Diffractometer (graphite monochromator, automatic gap, Cu K α radiation at $\lambda = 1.54061 \text{ \AA}$, powered at 45 kV–40 mA, and a scanning range of 4–100° with a 0.017°2 θ step scan and a measuring time of 50 s). Identification and Rietveld semiquantitative evaluation of phases were conducted with the PANalytical X’Pert HighScore software (PANalytical, Almelo, The Netherlands).

Scanning electron microscopy with energy-dispersive spectral analysis (SEM–EDS) was performed with a Hitachi TM-1000 tabletop electron microscope (EDX, High-Technologies Corporation, Tokyo, Japan).

Automated mineral liberation analysis (MLA) was used to study the particle liberation characteristics. Samples were prepared in thick sections and, to avoid the segregation of particles according to their densities [28], the round thick sections were cut into two vertical slices. Analyses were carried out at the University of Tasmania using a FEI MLA650 (FEI, Hillsboro, OR, USA) environmental scanning electron microscope equipped with

a Bruker Quantax Esprit 1.9 EDS system with two XFlash 5030 SDD detectors (Bruker, Berlin, Germany). MLA measurements were performed at 20 kV with a 1.5-micron pixel resolution using the XBSE method, which collects a range of BSE images at a specified resolution, segments the images into different mineral grains based on BSE contrast and textural features, and collects a single ED spectrum in the center of each identified mineral grain. A Mineral Liberation Analysis (MLA) software package v3.1 was used.

3. Results

3.1. Chemical Composition

The chemical composition of major components of dumps and tailings was previously reported [29]. A comparison of the chemistry of the feed tailings, concentrates, and final tailings from the Catavi plant is presented in Table 1. The contents of major elements were similar in the feed and final tailings, i.e., highly rich in SiO_2 and Al_2O_3 , with the most abundant oxide from the concentrate being SnO_2 . Fe, Ti, and P_2O_5 also were increased in the concentrated fraction.

Table 1. Chemical composition, in wt.%, of the tailings and processing products from the C-4 processing plant.

| Material | SiO_2 | Al_2O_3 | Fe_2O_3 | TiO_2 | MnO | CaO | K_2O | MgO | Na_2O | P_2O_5 | SnO_2 | LOI * |
|----------------|----------------|-------------------------|-------------------------|----------------|------|------|----------------------|------|-----------------------|------------------------|----------------|-------|
| Feed | 77.75 | 11.19 | 2.58 | 0.44 | 0.01 | 0.07 | 1.43 | 1.09 | 0.37 | 0.19 | 0.40 | 1.79 |
| Concentrate | 11.42 | 4.64 | 5.55 | 3.52 | 0.03 | 0.00 | 0.22 | 0.61 | 0.24 | 0.72 | 52.43 | 3.03 |
| Final tailings | 79.20 | 10.52 | 2.42 | 0.43 | 0.01 | 0.07 | 1.20 | 1.09 | 0.38 | 0.15 | 0.29 | 1.78 |

* LOI: loss on ignition.

The Sn content of the feed tailings varied between 0.40 and 1.7 wt.% [30]. After the concentration process using the shaking tables, the concentrate displayed 41.3% and 59.0 wt.% SnO_2 . The final tailings still contained relatively high amounts of Sn, between 0.23 and 0.37 wt.% SnO_2 . These contents are still of economic interest. The average grade for greisen-type tin deposits is 0.3% Sn [31].

The concentrate contained significant amounts of W, i.e., from 4990 to 6700 ppm, with 70 ppm remaining in the final tailings. The Pb content was 1560 ppm and Zn and Ag occurred in small amounts, i.e., 90 and 38 ppm, respectively.

There were also minor amounts of radioactive elements present, i.e., U in a range from 32 to 41 ppm and Th in a range from 66 and 80 ppm. Both contents were low in the final tailings, i.e., 3 and 6 ppm, respectively.

Indium occurs in relatively high concentrations in certain deposits of the Central Andean tin belt [32,33]. However, in Llallagua, the contents obtained were negligible, reaching only 0.03 ppm in the concentrate. Moreover, Nb and Ta were found in significant amounts in certain tin deposits, since they can replace Sn in the cassiterite structure [34]. However, in the case of the materials from Llallagua, the contents were low, i.e., 17 ppm and 12 ppm, respectively.

Other elements that are currently of great interest are germanium and gallium. In the materials from Llallagua, both were higher in the concentrate than in the final tailings. The concentrate had up to 9 ppm Ge and between 49 and 63 ppm Ga. The latter can be of interest as a by-product as this represents double the average content of Ga in the crust (10–20 ppm) and is similar to the amount found in bauxite ores, from where it is extracted as a by-product [35].

The concentrate contained a significant REE content, ranging between 8800 and more than 12,000 ppm of total REE (Table 2). The most abundant elements were cerium, lanthanum, and neodymium (Figure 4). On the other hand, the total rare earths were only 170 ppm in the final tailings. This indicates that most have been removed to the concentrate, leaving about 2% in the light fraction. An intermediate concentrate was also analyzed and, as expected, it contained fewer rare earths than the final concentrate, which indicates that,

at this stage, concentration had not been totally achieved. As expected, the intermediate concentrate had a lower rare earth content than the final concentrate.

Table 2. REE elements in the tailings and processing products from the C-4 plant, in ppm.

| Element | Final Tailings | Intermediate Concentrate | Final Concentrate 1 | Final Concentrate 2 |
|--------------|----------------|--------------------------|---------------------|---------------------|
| ppm | LG-2 | LG-4 | LG-35 | LG-41 |
| Ce | 74.5 | 3370 | 5670 | 4140 |
| Dy | 3.51 | 56.3 | 123 | 83.9 |
| Er | 1.72 | 19.1 | 47.6 | 30.1 |
| Eu | 1.09 | 31.5 | 56 | 40.3 |
| Gd | 3.86 | 109.5 | 210 | 144.5 |
| Ho | 0.63 | 8.5 | 18.9 | 13.05 |
| La | 37.2 | 1640 | 2860 | 2160 |
| Lu | 0.34 | 1.4 | 4.16 | 2.93 |
| Pr | 8.86 | 358 | 667 | 431 |
| Nd | 40.3 | 1250 | 2210 | 1520 |
| Sm | 5.48 | 185.5 | 366 | 251 |
| Tb | 0.6 | 13.3 | 23.3 | 16.85 |
| Tm | 0.25 | 2.1 | 5.81 | 3.75 |
| Yb | 1.74 | 11.3 | 32.7 | 21.8 |
| Σ RRE | 170.5 | 7056.5 | 12,294.5 | 8859.18 |

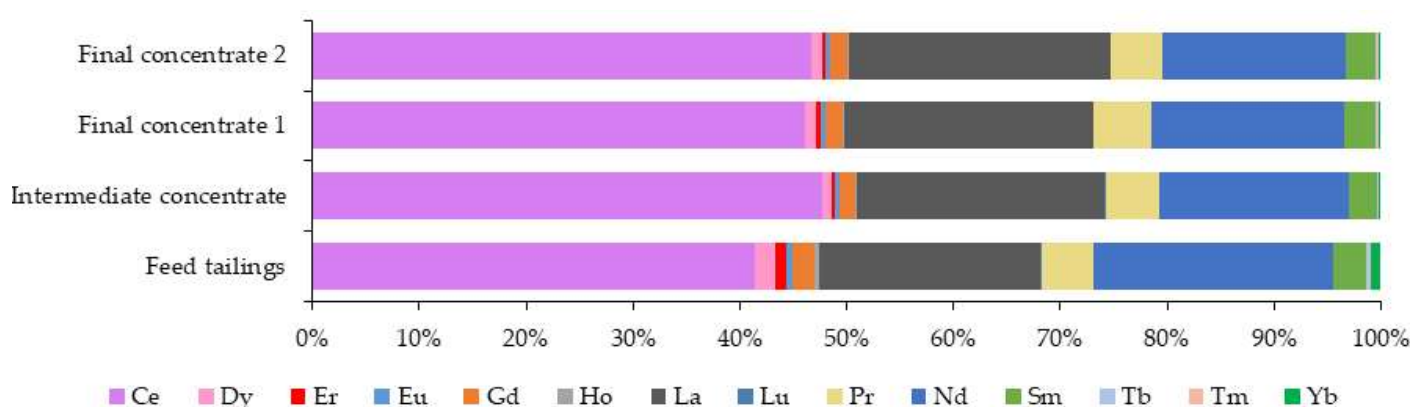


Figure 4. Ratios among the REE contents in the feed tailings and in the processing plant products.

3.2. Mineralogy

3.2.1. Major Minerals: XRD

The feed tailings were mainly composed of quartz and tourmaline of the dravite and schorl types, with minor amounts of micas. The micas were mainly sericite and illite. Muscovite, biotite, and highly altered feldspars were observed under the microscope, but they went undetected in the majority of XRD diffractograms. In the feed tailings, cassiterite was the most important metal oxide, although it was not abundant. In the final tailings, it was not present in sufficient amounts to be determined by XRD. After processing the material with shaking tables, the minerals of the feed tailings were grouped according to their densities, i.e., into a heavy fraction, or concentrate, and a light fraction, or final tailings (Figure 5).

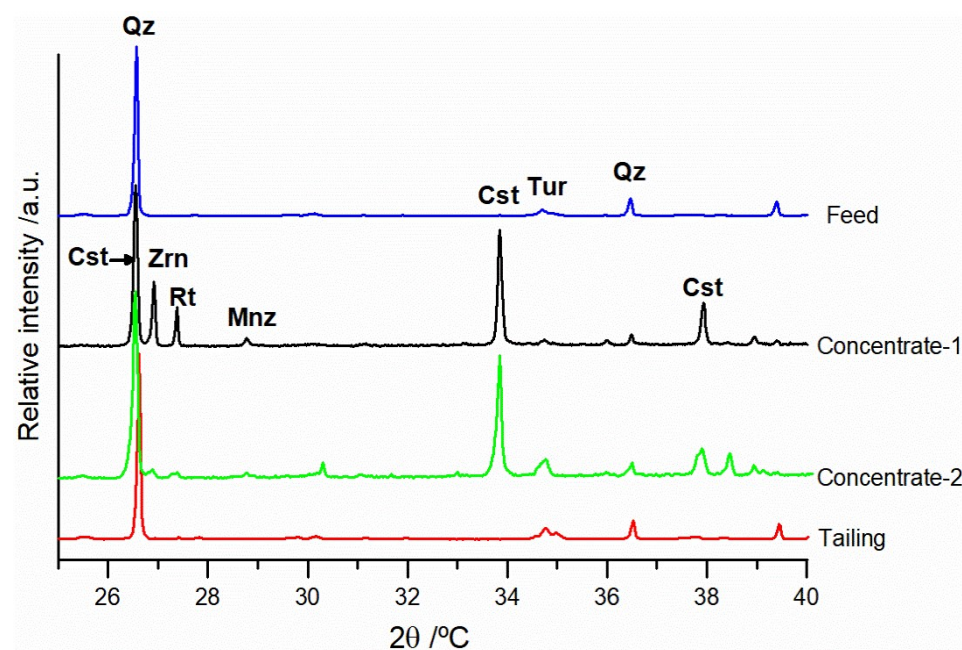


Figure 5. XRD diffractograms of materials from the Catavi processing plant. Qz: quartz; Tur: tourmaline; Cst: cassiterite; Zrn: zircon; Rt: rutile; Mnz: monazite.

Quartz was much more abundant in the final tailings. Tourmaline was also more abundant in the tailings, but with a less significant difference. The average density of tourmaline is 3.10 g/cm^3 , whereas that of quartz is 2.6 g/cm^3 . The floatability rates indicate that it is more difficult using gravity methods to separate tourmaline into the light fraction. Cassiterite was the predominant mineral in the concentrate. The semiquantitative determination using the Rietveld method provided a cassiterite content of 41–46 wt.%. A low intensity monazite peak can be observed in the concentrate diagram. The rutile and zircon contents were higher in the concentrates, although they can vary considerably according to the route followed during the processing, being up to 9 wt.% rutile and 9 wt.% zircon if the feed tailings were not floated (concentrate 1).

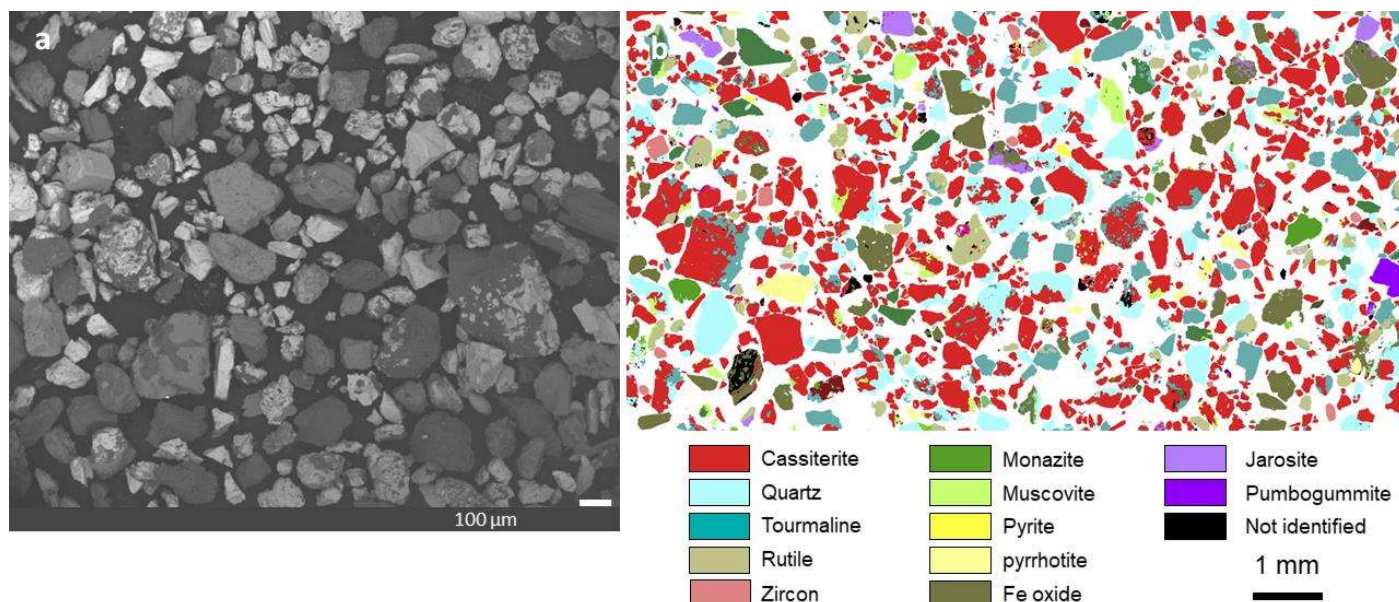
Most of the feed material remained in the final tailings; therefore, they demonstrated a mineralogical composition similar to that of the feed, with lower amounts of heavy minerals, such as cassiterite, rutile, zircon, and monazite.

3.2.2. Modal Mineralogy of the Concentrate

The mineralogy of the concentrate was also determined by MLA, which provided the modal estimation (Table 3). Cassiterite is the most abundant mineral in the concentrate, with 57.41 wt.%. This quantification is in accordance with the results of the chemical analyses; however, it is a contrast with the results obtained from XRD, in which the cassiterite contents were underestimated, probably because there is a superposition of the most intense peak reflections of cassiterite (at $d_{hkl} = 3.353 \text{ \AA}$) and quartz (at $d_{hkl} = 3.345 \text{ \AA}$). Zircon and rutile were also enriched in the concentrate. The MLA of concentrate 2 reported 0.69 wt.% of zircon. This is in accordance with the chemical composition results, i.e., 0.41 wt.% of Zr and 99 ppm of Hf, which corresponds to approximately 0.82 wt.% of zircon. In addition to Zr and Hf, this mineral probably contained a significant part of the U and Th determined in the chemical analysis of the concentrate. This mineral was frequently observed in the SEM as euhedral crystals with a homogeneous appearance or a slight zonation. The SEM observation and MLA map shows that in the concentrate, cassiterite only represented half of the components and most cassiterite particles were not completely liberated and contained some proportion of other minerals (Figure 6).

Table 3. Modal mineralogy provided by the MLA of concentrate 2 from Catavi.

| Mineral | Formula | wt % |
|-----------------|---|--------|
| Cassiterite | SnO_2 | 57.41 |
| Quartz | SiO_2 | 7.13 |
| Plagioclase | $(\text{Na,Ca})(\text{Si,Al})_4\text{O}_8$ | 0.02 |
| Tourmaline | $\text{Na}(\text{Mg,Fe})_3\text{Al}_6(\text{BO}_3)_3\text{Si}_6\text{O}_{18}(\text{OH})_4$ | 11.22 |
| Muscovite | $\text{KAl}_3\text{Si}_3\text{O}_{10}(\text{OH})_2$ | 1.41 |
| Biotite | $\text{KMg}_{2.5}\text{Fe}^{2+}_{0.5}\text{AlSi}_3\text{O}_{10}(\text{OH})_{1.75}\text{F}_{0.25}$ | 0.32 |
| Chlorite | $(\text{Mg,Fe})_3(\text{Si,Al})_4\text{O}_{10}(\text{OH})_2(\text{Mg,Fe})_3(\text{OH})_6$ | 0.09 |
| Kaolinite | $\text{Al}_2\text{Si}_2\text{O}_5(\text{OH})_4$ | 0.23 |
| Rutile | TiO_2 | 4.60 |
| Ilmenite | $\text{Fe}^{2+}\text{TiO}_3$ | 0.04 |
| Fe oxides | Fe_2O_3 | 10.44 |
| Pyrrhotite | FeS | 1.28 |
| Pyrite | FeS_2 | 0.37 |
| Arsenopyrite | FeAsS | 0.05 |
| Stannite | SnS | 0.01 |
| Galena | PbS | 0.01 |
| Crandallite | $\text{CaAl}_3(\text{PO}_4)_2(\text{OH})_5\text{H}_2\text{O}$ | 0.10 |
| Florencite | $\text{CeAl}_3(\text{PO}_4)_2(\text{OH})_6$ | 0.16 |
| Plumbogummite | $\text{PbAl}_3(\text{PO}_4)_2(\text{OH})_5(\text{H}_2\text{O})$ | 0.26 |
| Fe-Pb Phosphate | $(\text{Pb,Fe})_3(\text{PO}_4)_2$ | 0.33 |
| Scorodite | $\text{FeAsO}_4 \cdot 2(\text{H}_2\text{O})$ | 0.15 |
| Jarosite | $\text{KFe}_3(\text{SO}_4)_2(\text{OH})_6$ | 1.30 |
| Barite | $\text{Ba}(\text{SO}_4)$ | 0.14 |
| Xenotime | $\text{Y}(\text{PO}_4)$ | 0.04 |
| Monazite | $(\text{La,Ce,Nd,Th})(\text{PO}_4)$ | 1.62 |
| Zircon | ZrSiO_4 | 0.69 |
| Wolframite | $(\text{Fe,Mn})(\text{WO}_4)$ | 0.47 |
| Total | | 100.00 |

**Figure 6.** (a) SEM images of the concentrate 2 from Catavi; the lightest color is cassiterite. (b) False colour MLA map of the concentrate 2.

Iron oxides and hydroxides represented 10.44 wt.% and rutile 4.6 wt.%. Sulfides were not abundant, and pyrite pyrrhotite, arsenopyrite, galena, sphalerite and stannite occurred in minor amounts.

The REE-bearing phosphates were monazite and florencite. Monazite normally appears in idiomorphic crystals, with sizes of less than 100 μm , liberated or associated with tourmaline or quartz. Florencite was occasionally reported from Llallagua [15,26]. This is a crandallite-group REE-bearing phosphate that usually forms from the alteration of monazite [36]. Crandallite and plumbogummite were also determined by the MLA.

Sulfates, such as barite and jarosite, were also present in low amounts. Their presence has been confirmed by SEM observations.

3.3. Particle Size Distribution

The particle size distribution (PSD) data are used to predict the liberation size of ores and to determine the grinding parameters required to obtain an efficient recovery [37]. The PSD of the feed, concentrate, and final tailings was determined by laser analysis and the PSD of concentrate was additionally obtained by MLA. Both methods produced similar distribution curves. This indicates that the sample analyzed by MLA was representative of the different particle sizes. The MLA was expected to give a low particles size due to the stereological error associated with this technique [38,39]. However, in the C-4 plant concentrate, this lower size was not observed.

The particle size distribution shows that, in the feed and products of the Catavi plant, the number of finer particles was low (Figure 7a), i.e., only 5% of the population was less than 100 μm in the feed sands. After milling, the size reduction ratio in this finer phase was negligible. The feed tailings were the coarsest material and they were comminuted in the tumbling mills and the gravity separation produced a finer concentrate and coarser final tailings. This is because quartz, which is the main component of the tailings, is harder than cassiterite, which is the main product of the concentrate, with a Bond ball work index of 14–15 kWh/t in quartz compared to 10–12 kWh/t in cassiterite [40]. On the other hand, this could also be because cassiterite grains are originally smaller than quartz grains. In the concentrate, the grain size determined by MLA shows that the size of quartz was larger than that of cassiterite, monazite, and tourmaline (Figure 7b). Quartz grains reached up to 425 μm in diameter, accounting for 80 wt.% of the total of $-145 \mu\text{m}$. The cassiterite grain size was $-343 \mu\text{m}$, and 80 wt.% of the total was $-124 \mu\text{m}$. Monazite grains were $-203 \mu\text{m}$ in size, with 80 wt.% less than 106 μm .

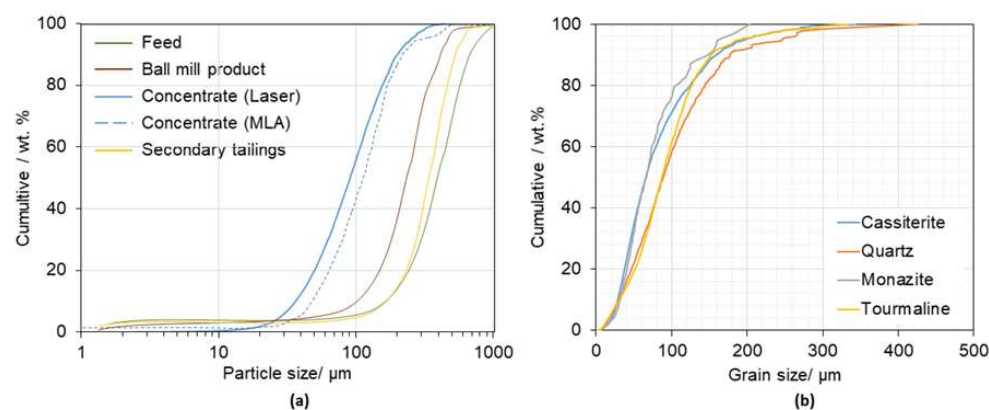


Figure 7. (a) Particle size of feed, concentrate and tailings from the Catavi plant, (b) Grain size of the minerals from the concentrate.

3.4. Mineral Liberation

The liberation characteristics of the concentrate were determined from the data provided by the MLA. The degree of liberation and the association among minerals could be established. These characteristics were determined in the minerals that constitute or may constitute ores, that is, cassiterite and minerals that contain rare earths, which in this case, were monazite, xenotime, and florencite.

The total number of particles analyzed in the MLA of the concentrate was 49,386 and 85,378 grains. Of these, there were 24,794 grains of cassiterite, 1190 of monazite, 88 of xenotime and 779 of florencite. The liberation characteristics of cassiterite and monazite in the concentrate of the Catavi plant are summarized in Table 4.

Table 4. Characteristics of ore-bearing particles from concentrate 2 of the C-4 plant.

| | Cassiterite | Monazite |
|--|-------------|----------|
| Total ore (wt %) | 57.41 | 1.62 |
| Number of particles | 24,794 | 1190 |
| Particles contain% | 50.20 | 2.41 |
| Number of liberated particles | 19,708 | 586 |
| Mass liberated respect the total ore % | 65.74 | 63.83 |
| Mass liberated respect the total concentrate % | 37.74 | 1.03 |

3.4.1. Cassiterite

Cassiterite represented 57.41 wt.% of the total mass of the concentrate and 50.2% of the concentrated particles contained cassiterite. More than half of the cassiterite in the concentrate was liberated, i.e., 65.74 wt.% of the total cassiterite ore, which represents 37.74 wt.% of the total mass of the concentrate. Moreover, 24.28 wt.% of the non-liberated cassiterite grains occurred in binary particles and 9.99 wt.% occurred in ternary particles. As regards being associated with other minerals as binary and ternary particles, cassiterite was mainly in contact with quartz, tourmaline, rutile, and muscovite. This was already demonstrated in the SEM observations (Figures 8 and 9). In addition, the MLA allowed us to quantify these observations and determine the minor associations (Table 3).

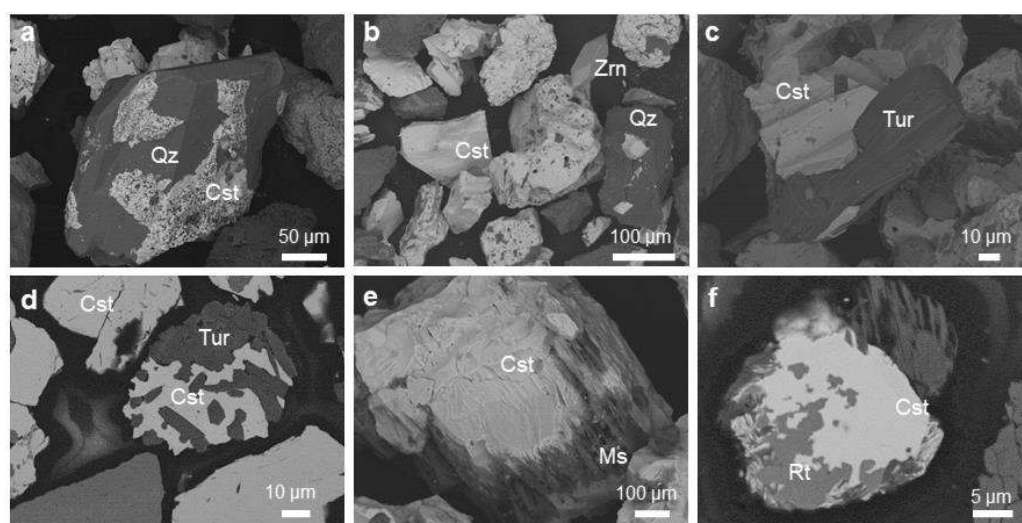


Figure 8. Images of the mineral association of binary particles of cassiterite in the concentrate from Catavi: (a,b) with quartz, (c,d) with tourmaline, (e) with muscovite, and (f) with rutile. Qz: quartz; Cst: cassiterite; Tur: tourmaline; Ms: muscovite; Rt: rutile.

3.4.2. Monazite

Monazite represented 1.62 wt.% of the total concentrate. In addition, 2.41% of the concentrated particles contained monazite and 63.83 wt.% of the total monazite was liberated, which represented 1.03 wt.% of the concentrate. The non-liberated monazite was mainly associated with cassiterite, tourmaline, and quartz, followed by rutile and zircon (Figure 9).

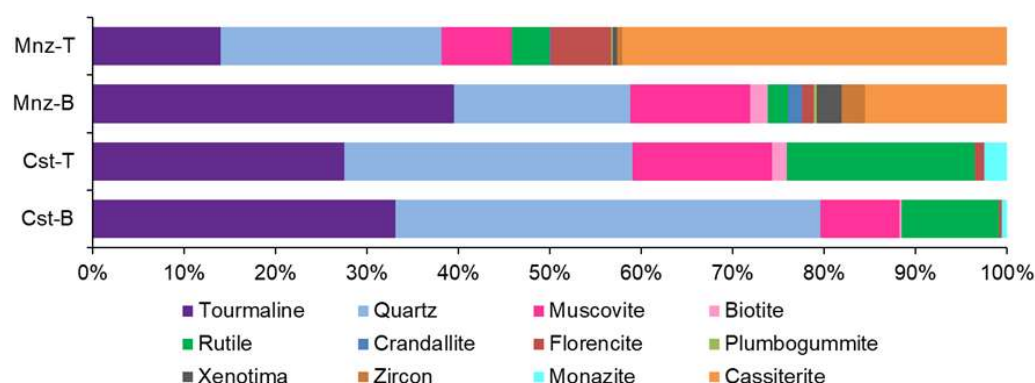


Figure 9. Mineral association of the non-liberated ore: Cst-B cassiterite in binary particles, Cst-T cassiterite in ternary particles, Mnz-B monazite in binary particles and Mnz-T monazite in ternary particles.

4. Discussion

The grinding process moderately reduced the size of the sands that constituted the feed tailings, which exhibited an average particle size of 540 μm . On the other hand, the average size of the cassiterite and monazite grains was 66 μm . Therefore, after grinding, one part of the ore remained unliberated. The analysis of cassiterite liberation by grade ranges is shown in Figure 10. A significant amount of cassiterite was found in mixed particles, with 65.73% of it being liberated.

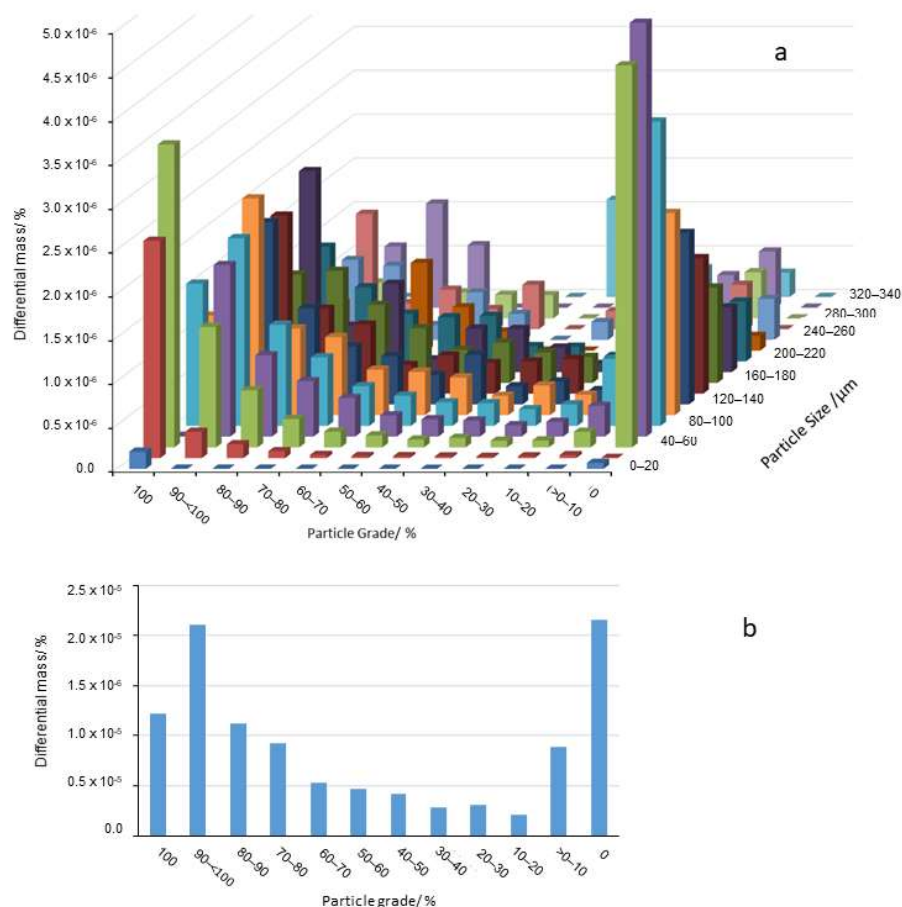


Figure 10. Distribution of cassiterite in the concentrated materials: (a) according to particle size and cassiterite grade classes; (b) according to the grade.

The distribution of the concentrate into the different particle sizes shows that the concentrate contained a low number of particles of less than 40 μm . Moreover, it shows

that most particles of this class can be considered liberated cassiterite. Particles larger than +80 μm were mainly mixed. The most abundant content of cassiterite-free particles in the concentrate was in the size classes of +60 to +180 μm . This could be indicative of a loss of ore in the finest fractions during processing. This behavior was also reported in other cases, with the lack of fine cassiterite particles in the concentrate being attributed to an aqua flow phenomenon [40,41].

In the case of monazite, the distribution of the concentrate into the different particle sizes shows that there are few particles of liberated monazite less than 40 μm in size, with the most abundant content of liberated monazite particles occurring in the size class between 60 and 80 μm . The lower content of high-grade liberated monazite particles in the finer class size could be due to the fact that they are associated with cassiterite (Figure 11).

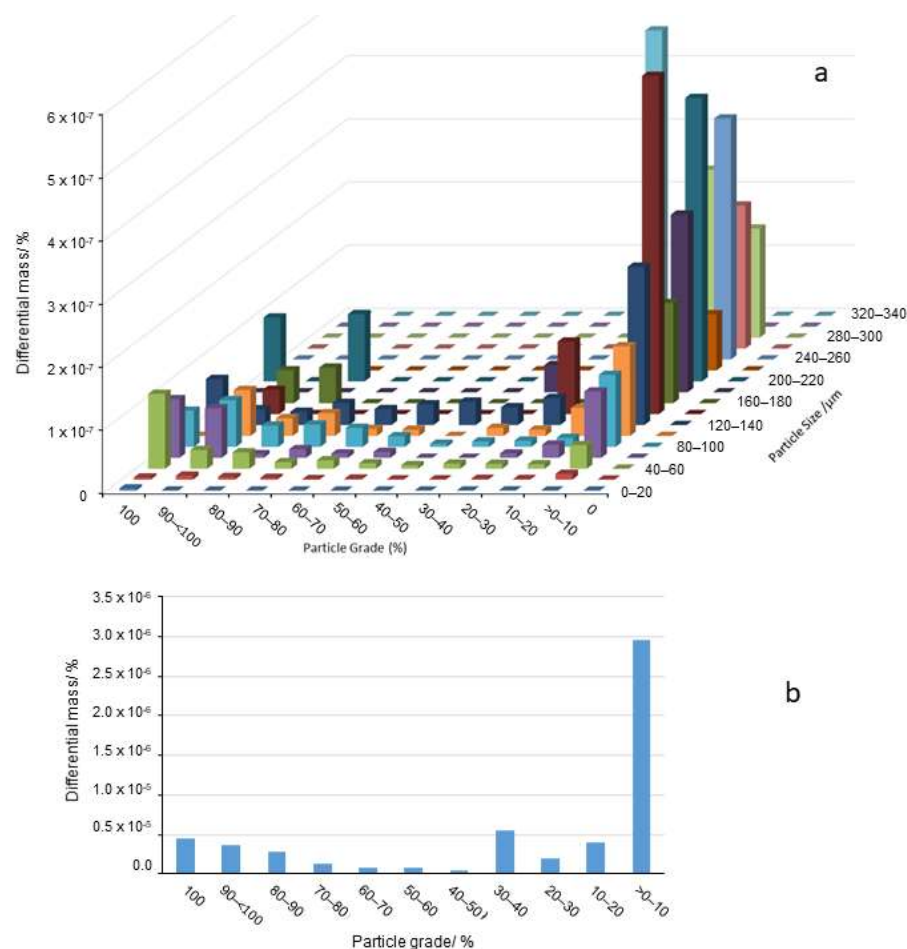


Figure 11. Distribution of monazite in the concentrated materials: (a) according to particle size and cassiterite grade classes; (b) according to the grade. The zero grade particles are not shown.

Therefore, particle size reduction should be necessary to increase the liberation and, consequently, the recovery of cassiterite and increase its grade in the concentrate. A high amount of energy is consumed during the comminution process, which means that when a significant size reduction is required, a large expense is also required [42]. An alternative could be the use of high-pressure grinding rolls (HPGR) before milling in the ball mill. This may represent an economical solution since HPGR produce a high number of micro-fractures in the material, which facilitates the increase in the liberation with a moderate size reduction [43]. Additionally, the grinding media charge and the increase in residence times should also be considered [44].

The REE content in the concentrate from Llallagua feed tailings (between 8859 and 12,294 ppm) is sufficient to be considered a suitable by-product of Sn production. The higher

amount corresponds to samples that were not floated. In this case, the floated concentrate was also depleted in rutile and zircon as compared to the non-floated sample. Then, the flotation part of REE was floated with sulfide minerals, rutile, and zircon. The flotation of monazite-rich samples should be taken into account in the flow diagram, considering the inclusion of the flotation process or changing the depressants used, according to existing studies [45].

In other cases, lower REE concentrations in tailings were considered of interest, as was the case of the Kiirunavaara iron deposit [46] and in a copper flotation plant of Australia [47]. Other tin mining activities consider REE of interest for recovery as a by-product [48,49], such as thorium-rich monazite from Malaysia [50]. In contrast to this example, monazite from Llallagua has the advantage of being Th-poor [14–16].

5. Conclusions

The reprocessing of the sandy tailings from the Catavi plant produced final tailings with about 0.29 wt.% SnO₂, which is rich enough to be of economic interest. To make the mining activity of Llallagua more sustainable, Sn losses must be reduced. To this end, recovery needs to be improved. The average liberation size of cassiterite was 66 µm, whereas that of the feed tailings was 540 µm. Finer particle size of the processed tailings is necessary to increase the liberation and recovery of Sn, and the cassiterite grade of the concentrate. It is evident that the efficiency of the mill is very low, and the comminution process should be improved. To this end, the control of the grinding media charge and the residence times should be studied. Using different combinations of equipment also demonstrated that other techniques may increase the reduction ratios.

In addition, there was a significant amount of REE in the concentrate, i.e., between 8859 and 12,294 ppm of total REE, which is of economic interest as a by-product. REE occurred mainly as monazite, and florencite, with minor amounts of xenotime. The density of these phosphate minerals is moderate, making their separation from the concentrate by gravitational separation methods difficult. Therefore, future studies should attempt to identify an optimal method to recover this ore should be recovered during the metallurgic process.

Author Contributions: Conceptualization, P.A. and M.R.; methodology, P.A.; Field work: P.A., M.R., R.N.Z., A.S.; software, P.A.; M.G.-V.; validation, P.A., H.A. and M.R.; formal analysis, M.G.-V., M.S.; investigation, P.A., M.S., H.A., N.S.-R.; resources, P.A., M.G.-V.; data curation, P.A.; writing—original draft preparation, P.A.; writing—review and editing, P.A., M.R., M.G.-V., H.A., N.S.-R.; supervision, P.A.; project administration, P.A.; funding acquisition, P.A. All authors have read and agreed to the published version of the manuscript.

Funding: This research was funded by the Centre de Cooperació al desenvolupament de la Universitat Politècnica de Catalunya, grant number 2018-U017 and 2019-B005.

Data Availability Statement: Not applicable.

Acknowledgments: We acknowledge at Multiactiva Catavi-Siglo XX cooperative the access to the processing plant and help in the sampling.

Conflicts of Interest: The authors declare no conflict of interest.

References

1. Edraki, M.; Baumgartl, T.; Manlapig, E.; Bradshaw, D.; Franks, D.M.; Moran, C.J. Designing mine tailings for better environmental, social and economic outcomes: A review of alternative approaches. *J. Clean. Prod.* **2004**, *84*, 411–420. [[CrossRef](#)]
2. Khan, M.M.; Mahajani, S.M.; Jadhav, G.N.; Vishwakarma, R.; Malgaonkar, V.; Mandre, S. Mechanical and thermal methods for reclamation of waste foundry sand. *J. Environ. Manag.* **2021**, *279*, 111628. [[CrossRef](#)] [[PubMed](#)]
3. Asr, E.T.; Kakaie, R.; Ataei, M.; Mohammadi, M.R.T. A review of studies on sustainable development in mining life cycle. *J. Clean. Prod.* **2019**, *229*, 213–231. [[CrossRef](#)]
4. Laurence, D. Establishing a sustainable mining operation: An overview. *J. Clean. Prod.* **2011**, *19*, 278–284. [[CrossRef](#)]
5. United Nations. The future We Want. In Proceedings of the United Nations Conference on Sustainable Development, Rio de Janeiro, Brazil, 20–22 June 2012.

6. Dold, B. Sustainability in metal mining: From exploration, over processing to mine waste management. *Rev. Environ. Sci. Biotechnol.* **2008**, *7*, 275–285. [\[CrossRef\]](#)
7. Ahlfeld, F. The tin deposits of Llallagua, Bolivia. *Econ. Geol.* **1936**, *31*, 219–221. [\[CrossRef\]](#)
8. Ahlfeld, F.; Schneider-Scherbina, A. Los yacimientos minerales y de hidrocarburos de Bolivia. *Bol. Dept. Nac. Geol.* **1964**, *5*, 1–388.
9. Hyrsl, J.; Petrov, A. Famous mineral localities: Llallagua, Bolivia. *Mineral. Rec.* **2006**, *37*, 17–163.
10. Zambrana, R.N. Retratamiento de Colas Finales Planta C-4 de Catavi y Propuesta Técnica Económica y Ambiental. Master's Thesis, Universitat Politècnica de Catalunya, Manresa, Spain, 2011.
11. Villalpando, B.A. The tin ore deposits of Bolivia. In *Geology of Tin Deposits in Asia and the Pacific*; Hutchinson, C.S., Ed.; Springer: Berlin/Heidelberg, Germany, 1988; pp. 201–215.
12. Romero, F.M.; Canet, C.; Alfonso, P.; Zambrana, R.N.; Soto, N. The role of cassiterite controlling arsenic mobility in an abandoned stanniferous tailings impoundment at Llallagua, Bolivia. *Sci. Total Environ.* **2014**, *481*, 100–107. [\[CrossRef\]](#)
13. Kempe, U.; Lehmann, B.; Wolf, D.; Rodionov, N.; Bombach, K.; Schwengfelder, U.; Dietrich, A. U–Pb SHRIMP geochronology of Th-poor, hydrothermal monazite: An example from the Llallagua tin-porphyry deposit, Bolivia. *Geochim. Cosmochim. Acta* **2008**, *72*, 4352–4366. [\[CrossRef\]](#)
14. Catlos, E.J.; Miller, N.R. Speculations Linking Monazite Compositions to Origin: Llallagua Tin Ore Deposit (Bolivia). *Resources* **2017**, *6*, 36. [\[CrossRef\]](#)
15. Betkowski, W.B.; Rakovan, J.; Harlov, D.E. Geochemical and textural characterization of phosphate accessory phases in the vein assemblage and metasomatically altered Llallagua tin porphyry. *Mineral. Petrol.* **2017**, *111*, 547–568. [\[CrossRef\]](#)
16. Zglinicki, K.; Szamalek, K.; Konopka, G. Monazite-bearing post processing wastes and their potential economic significance. *Miner. Resour. Manag.* **2020**, *36*, 37–58.
17. Zhou, B.; Li, Z.; Chen, C. Global potential of rare earth resources and rare earth demand from clean technologies. *Minerals* **2017**, *7*, 203. [\[CrossRef\]](#)
18. Massari, S.; Ruberti, M. Rare earth elements as critical raw materials: Focus on international markets and future strategies. *Resour. Policy* **2013**, *38*, 36–43. [\[CrossRef\]](#)
19. European Commission. Study on the Review of the List of Critical Raw Materials: 546 Executive Summary. European Commission, Directorate-General for Internal Market, 547 Industry, Entrepreneurship and SMEs. Available online: <https://publications.europa.eu/en/publication548detail/-/publication/08fdab5f-9766-11e7-b92d-01aa75ed71a1/language-en> (accessed on 15 November 2021).
20. Binnemans, K.; Jones, P.T.; Blanpain, B.; Van Gerven, T.; Pontikes, Y. Towards zero-waste valorisation of rare-earth-containing industrial process residues: A critical review. *J. Clean. Prod.* **2015**, *99*, 17–38. [\[CrossRef\]](#)
21. Pereira, L.; Birtel, S.; Möckel, R.; Michaux, B.; Silva, A.C.; Gutzmer, J. Constraining the economic potential of by-product recovery by using a geometallurgical approach: The example of rare earth element recovery at Catalão I, Brazil. *Econ. Geol.* **2019**, *114*, 1555–1568. [\[CrossRef\]](#)
22. Sillitoe, R.H.; Halls, C.; Grant, J.N. Porphyry tin deposits in Bolivia. *Econ. Geol.* **1975**, *70*, 913–927. [\[CrossRef\]](#)
23. Dietrich, A.; Lehmann, B.; Wallianos, A. Bulk Rock and melt inclusion geochemistry of Bolivian tin porphyry systems. *Econ. Geol.* **2000**, *95*, 313–326. [\[CrossRef\]](#)
24. Grant, J.N.; Halls, C.; Ávila Salinas, W.; Snelling, N.J. K–Ar ages of igneous rocks and mineralization in part of the Bolivian tin belt. *Econ. Geol.* **1979**, *74*, 838–851. [\[CrossRef\]](#)
25. Lehmann, B. Petrochemical factors governing the metallogeny of the Bolivian tin belt. In *Tectonics of the Southern Central Andes, Structure and Evolution of an Active Continental Margin*; Reutter, K.J., Scheuber, E., Wigger, P., Eds.; Springer: Berlin, Germany, 1994; pp. 317–326.
26. Grant, J.N.; Halls, C.; Avila, W.; Avila, G. Igneous geology and the evolution of hydrothermal systems in some subvolcanic tin deposits of Bolivia. *Geol. Soc. Lond. Spec. Publ.* **1977**, *7*, 117–126. [\[CrossRef\]](#)
27. Mlynarczyk, M.; Williams-Jones, A.E. The role of collisional tectonics in the metallogeny of the central Andean tin belt. *Earth Planet Sci. Lett.* **2005**, *240*, 656–667. [\[CrossRef\]](#)
28. Schulz, B.; Sandmann, D.; Gilbricht, S. SEM-Based Automated Mineralogy and Its Application in Geo- and Material Sciences. *Minerals* **2020**, *10*, 1004. [\[CrossRef\]](#)
29. Arancibia, J.R.H.; Alfonso, P.; García-Valles, M.; Martínez, S.; Canet, C.; Romero, F.M. Obtención de vidrio a partir de residuos de la minería del estaño en Bolivia. *Bol. Soc. Esp. Ceram. Vidr.* **2013**, *52*, 143–150. [\[CrossRef\]](#)
30. Menzie, W.D.; Reed, B.L.; Singer, D.A. Models of grades and tonnages of some lode tin deposits. In *Geology of Tin Deposits in Asia and the Pacific*; Springer: Berlin/Heidelberg, Germany, 1988; pp. 73–88.
31. Ishihara, S.; Murakami, H.; Marquez-Zavalia, M.F. Inferred indium resources of the Bolivian tin-polymetallic deposits. *Resour. Geol.* **2011**, *61*, 174–191. [\[CrossRef\]](#)
32. Jiménez-Franco, A.; Alfonso, P.; Canet, C.; Trujillo, J.E. Mineral chemistry of In-bearing minerals in the Santa Fe mining district, Bolivia. *Andean Geol.* **2018**, *45*, 410–432. [\[CrossRef\]](#)
33. Torró, L.; Melgarejo, J.C.; Gemmrich, L.; Mollinedo, D.; Cazorla, M.; Martínez, Á.; Artiaga, D.; Torres, B.; Alfonso, P.; Arce, O. Spatial and Temporal Controls on the Distribution of Indium in Xenothermal Vein-Deposits: The Huari Huari District, Potosí, Bolivia. *Minerals* **2019**, *9*, 304. [\[CrossRef\]](#)

34. Alfonso, P.; Garcia-Valles, M.; Llorens, T.; Tomasa, O.; Calvo, D.; Guasch, E.; Anticoi, H.; Oliva, J.; López Moro, J.; García Polonio, F. Nb-Ta mineralization from the rare element granite from Penouta, Galicia, Spain. *Mineral. Mag.* **2018**, *82*, S199–S222. [\[CrossRef\]](#)
35. Gray, F.; Kramer, D.A.; Bliss, J.D. *Gallium and Gallium Compounds*; Wiley-VCH Verlag GmbH & Co. KGaA: Weinheim, Germany, 2000; ISBN 978-3-527-30673-2.
36. Mordberg, L.E.; Stanley, C.J.; Germann, K. Rare earth element anomalies in crandallite group minerals from the Schugorsk bauxite deposit, Timan, Russia. *Eur. J. Mineral.* **2000**, *12*, 1229–1243. [\[CrossRef\]](#)
37. Evans, C.L.; Napier-Munn, T.J. Estimating error in measurements of mineral grain size distribution. *Miner. Eng.* **2013**, *52*, 198–203. [\[CrossRef\]](#)
38. Spencer, S.; Sutherland, D. Stereological correction of mineral liberation grade distributions estimated by single sectioning of particles. *Image Anal. Stereol.* **2000**, *19*, 175–182. [\[CrossRef\]](#)
39. Ueda, T.; Oki, T.; Koyanaka, S. Comparison of seven texture analysis indices for their applicability to stereological correction of mineral liberation assessment in binary particle systems. *Minerals* **2017**, *7*, 222. [\[CrossRef\]](#)
40. Gupta, A.; Yan, D. *Mineral Processing Design and Operations: An Introduction*; Elsevier: Amsterdam, The Netherlands, 2016; pp. 563–628.
41. Bru, K.; Sousa, R.; Leite, M.M.; Broadbent, C.; Stuart, G.; Pashkevich, D.; Martin, M.; Kern, M.; Parvaz, D.B. Pilot-scale investigation of two Electric Pulse Fragmentation (EPF) approaches for the mineral processing of a low-grade cassiterite schist ore. *Miner. Eng.* **2020**, *150*, 106270. [\[CrossRef\]](#)
42. Abouzeid, A.Z.M.; Fuerstenau, D.W. Grinding of mineral mixtures in high-pressure grinding rolls. *Int. J. Miner. Process.* **2009**, *93*, 59–65. [\[CrossRef\]](#)
43. Hamid, S.A.; Alfonso, P.; Anticoi, H.; Guasch, E.; Oliva, J.; Dosbaba, M.; Garcia-valles, M.; Chugunova, M. Quantitative mineralogical comparison between HPGR and ball mill products of a Sn-Ta ore. *Minerals* **2018**, *8*, 151. [\[CrossRef\]](#)
44. Genç, Ö. Analysis of grinding media effect on specific breakage rate function of particles in a full-scale open circuit three-compartment cement ball mill. *Miner. Eng.* **2015**, *81*, 10–17. [\[CrossRef\]](#)
45. Nduwa-Mushidi, J.; Anderson, C.G. Surface Chemistry and Flotation Behaviors of Monazite–Apatite–Ilmenite–Quartz–Rutile–Zircon with Octanohydroxamic Acid. *J. Sustain. Metall.* **2017**, *3*, 62–72. [\[CrossRef\]](#)
46. Wanhainen, C.; Pålsson, B.I.; Martinsson, O.; Lahaye, Y. Rare earth mineralogy in tailings from Kiirunavaara iron ore, northern Sweden: Implications for mineral processing. *Miner. Metall. Processing* **2017**, *34*, 189–200. [\[CrossRef\]](#)
47. Abaka-Wood, G.B.; Addai-Mensah, J.; Skinner, W. The Use of Mining Tailings as Analog of Rare Earth Elements Resources: Part 1—Characterization and Preliminary Separation. *Miner. Process. Extr. Metall. Rev.* **2021**, 1–15. [\[CrossRef\]](#)
48. Alves, F.E.; Neumann, R.; Ávila, C.A.; Ferreira, P.E.; Assumpção, C.D.S.; Carneiro, M.C.; Garcia, P.H. Mineralogical auditing of the Volta Grande Mine (SE Brazil) Sn-Ta-Nb-Li processing plant, aiming at REE recovery as by-products. *Appl. Earth Sci.* **2021**, *130*, 198–208. [\[CrossRef\]](#)
49. Adiputra, R.N.; Agustin, F.; Sulastri, A.; Abdullah, C.I.; Nugraha, I.; Andriansyah, R.; Hadiprayitno, M. The tin ore separation process and optimizing the rare earth mineral (monazite) as a by-product of tin mining in East Belitung Regency. *IOP Conf. Ser. Earth Environ. Sci.* **2020**, *413*, 012004, IOP Publishing. [\[CrossRef\]](#)
50. Udayakumar, S.; Noor, A.F.M.; Hamid, S.A.R.S.A.; Putra, T.A.R.; Anderson, C.G. Chemical and mineralogical characterization of Malaysian monazite concentrate. *Min. Metall. Explor.* **2020**, *37*, 415–431. [\[CrossRef\]](#)